

SHORT COMMUNICATION

Pressure-induced structural transition of mature HIV-1 protease from a combined NMR/MD simulation approach

Julien Roche, John M. Louis, Ad Bax, and Robert B. Best*

Laboratory of Chemical Physics, National Institute of Diabetes and Digestive and Kidney Diseases, National Institutes of Health, Bethesda, Maryland 20892

ABSTRACT

We investigate the pressure-induced structural changes in the mature human immunodeficiency virus type 1 protease dimer, using residual dipolar coupling (RDC) measurements in a weakly oriented solution. $^1\text{D}_{\text{NH}}$ RDCs were measured under high-pressure conditions for an inhibitor-free PR and an inhibitor-bound complex, as well as for an inhibitor-free multidrug resistant protease bearing 20 mutations (PR20). While PR20 and the inhibitor-bound PR were little affected by pressure, inhibitor-free PR showed significant differences in the RDCs measured at 600 bar compared with 1 bar. The structural basis of such changes was investigated by MD simulations using the experimental RDC restraints, revealing substantial conformational perturbations, specifically a partial opening of the flaps and the penetration of water molecules into the hydrophobic core of the subunits at high pressure. This study highlights the exquisite sensitivity of RDCs to pressure-induced conformational changes and illustrates how RDCs combined with MD simulations can be used to determine the structural properties of metastable intermediate states on the folding energy landscape.

Proteins 2015; 00:000–000.

Published 2015. This article is a U.S. Government work and is in the public domain in the USA.

Key words: protein folding and stability; high-pressure; packing defects; conformational fluctuations; cavities; ubiquitin.

INTRODUCTION

High-pressure NMR has emerged as a powerful technique to characterize low lying protein intermediate states,¹ which are notoriously difficult to identify and characterize in the absence of perturbation.² A wide range of NMR techniques has been used over the past years to identify and characterize such low-lying intermediate states populated at elevated pressures, including ^{15}N relaxation,³ R_2 relaxation dispersion,⁴ $^1\text{H}/^2\text{H}$ exchange,^{5,6} J-coupling measurements,^{7,8} and chemical shift perturbation.⁹ Notably, the structure of a high-pressure intermediate state of ubiquitin has been studied based on a set of NOE distances and torsion angle restraints measured at 3000 bar.¹⁰

Despite their widespread use for the refinement and validation of high-resolution protein structures,^{11,12} and early measurements of residual dipolar coupling (RDC)

changes with pressure for the cold shock protein CspTm,¹³ RDCs have not yet been employed successfully for the characterization of intermediate states at high pressure. RDCs can be measured by inducing a very slight deviation from the random, isotropic distribution of macromolecules in an NMR sample and are exquisitely sensitive reporters of the time-averaged orientation

Additional Supporting Information may be found in the online version of this article.

Grant sponsor: Intramural Research Program of the National Institute of Diabetes and Digestive and Kidney Diseases of the National Institutes of Health; Grant sponsor: Intramural AIDS Research Fellowship.

*Correspondence to: Robert B. Best, Laboratory of Chemical Physics, National Institute of Diabetes and Digestive and Kidney Diseases, National Institutes of Health, Bethesda, MD 20892. E-mail: robertbe@helix.nih.gov

Received 28 July 2015; Revised 1 September 2015; Accepted 1 September 2015
Published online 18 September 2015 in Wiley Online Library (wileyonlinelibrary.com). DOI: 10.1002/prot.24931

of the corresponding inter-nuclear vectors,¹² providing powerful restraints for structure determination.¹⁴ Our measurement of $^1D_{NH}$ backbone RDCs for ubiquitin in a dilute solution of Pf1 filamentous phage revealed excellent agreement with the reference high-resolution structure of ubiquitin over a wide range of pressures from 1 bar to 2500 bar (Supporting Information Fig. S1), providing strong evidence for the absence of any significant pressure-induced structural change over this pressure range. When measured at high accuracy, the exquisite sensitivity of RDCs to even minute structural changes highlights their utility for structural characterization of high-pressure intermediate states. However, our results for ubiquitin also demonstrate that a change in RDC does not directly equate with a change in average backbone structure as the alignment tensor generally will be pressure dependent.

The use of RDCs as structural restraints to assist the conformational sampling in all-atom molecular dynamics simulations has also recently emerged as a powerful method to obtain detailed structural models of proteins in denatured, intermediate and transition states.^{15–17} In addition, all-atom MD simulations can capture the pressure-dependence of protein stability.¹⁸

Here, we introduce a strategy that combines the measurement of RDCs under high-pressure conditions with all-atom MD simulations to study the effects of pressure on human immunodeficiency virus type 1 protease dimer (HIV-1 PR) near the midpoint of the unfolding transition. The HIV-1 PR is a homodimeric aspartic hydrolase with 99 amino acids in each subunit. Each monomer contains a glycine-rich flap segment (residue 44–57), known to be essential to the catalytic activity of PR.¹⁹ In a recent study,²⁰ we determined the preferred flap orientations of PR in solution by measuring RDCs for the backbone amide N–H vectors of an inhibitor-free PR and a symmetric inhibitor DMP323-bound complex,²¹ as well as for an inhibitor-free multidrug resistant variant PR20.²² The RDC data clearly indicate that the inhibitor-free protease, on average, adopts a closed conformation in solution that is very similar to the inhibitor-bound state. By contrast, PR20 adopts a wide-open flap conformation.²⁰

MATERIALS AND METHODS

Experimental

The protease constructs used in this study contained the active site D25N mutation to prevent autoproteolysis.²³ The D25N mutation was introduced into the mature PR20 template, a protease inhibitor resistant clinical isolate,²² by employing the Quik-Change mutagenesis protocol (Agilent Technologies, Santa Clara, CA). Cells were grown in M9 minimal medium containing 0.5 g/L $^2H/^{15}N/^{13}C$ Isogro (Sigma-Aldrich), 2H_2O , 1.2 g/L $^{15}NH_4Cl$, and 2 g/L $^2H_7,^{13}C_6$ -D-glucose for

$^2H/^{15}N/^{13}C$ -labeling and expression was induced at an optical density of 0.7 (600 nm) with a final concentration of 1 mM isopropyl β -D-1-thiogalactopyranoside (IPTG) for a period of 4 h.

Cells harvested from 1 L of culture were suspended in 70 mL of buffer A [50 mM Tris-HCl, pH 8, 10 mM ethylenediaminetetraacetic acid (EDTA), and 10 mM dithiothreitol (DTT)], followed by the addition of lysozyme (100 μ g mL⁻¹) and sonicated at 4°C. The insoluble recombinant protein was washed by resuspension and brief sonication in 70 mL of buffer containing 50 mM Tris-HCl, pH 8, 10 mM EDTA, 10 mM DTT, 2M urea, and 1% Triton X-100 and subsequently in buffer A. In all cases, the insoluble fraction was pelleted by centrifugation at 20,000g for 30 min at 4°C. The final pellet was solubilized in 50 mM Tris-HCl, pH 8.0, 7.5M guanidine hydrochloride (GdHCl), 5 mM EDTA, and 10 mM DTT to yield a concentration of \sim 20 mg mL⁻¹. A maximum of 18 mg of protein was loaded on a Superdex-75 column (HiLoad 1.6 \times 60 cm², GE HealthCare, Piscataway, NJ) equilibrated in 50 mM Tris-HCl, pH 8, 4M GdHCl, 5 mM EDTA, and 1 mM DTT at a flow rate of 1.4 mL min⁻¹ at ambient temperature. Peak fractions were analyzed by SDS-PAGE, pooled, and subjected to reverse-phase HPLC (POROS 20 R2, Life Technologies, Grand Island, NY). The protein was eluted using a linear gradient from 99.95% water (v/v) and 0.05% TFA to 60% acetonitrile (v/v), 0.05% TFA (v/v), and 39.95% water (v/v) over a period of 16 min at a flow rate of 4 mL min⁻¹. Peak fractions were combined, estimated for protein content at 280 nm, analyzed by SDS-PAGE and stored at -70° C.

A fraction of the pure protein was dialyzed against HCl (12 mM), concentrated and stored at 4°C. Typically, proteins were refolded by dilution of the stock solution in 6.6 volumes of acetate buffer (5 mM, pH 6.0), with (five-fold molar excess) or without DMP323 inhibitor, and then were dialyzed extensively in 20 mM sodium phosphate (pH 5.7) and concentrated.

The $^1D_{NH}$ RDCs were derived from the difference in $^1J_{NH} + ^1D_{NH}$ splitting measured at 600 MHz using an ARTSY-HSQC experiment²⁴ on an isotropic sample and an aligned sample. All experiments were performed at 293 K. The alignment of the samples was obtained by the addition of 10 mg mL⁻¹ squalamine and 5 mM hexan-1-ol, yielding a stable lock solvent 2H quadrupole splitting of \sim 22 Hz. The average experimental error in the measured $^1D_{NH}$ RDCs was 0.15 Hz. For all the experiments described above, a commercial ceramic high-pressure NMR cell and an automatic pump system (Daedalus Innovations, Philadelphia, PA) was used to vary the pressure in the 1–2500 bar range.

Simulations

Simulations were run using Gromacs 4.5.5²⁵ using the Amber ff99SBws force field,^{26,27} initialized from the

3BVB crystal structure.²³ Lennard-Jones interactions were evaluated with a twin range cut-off scheme in which interaction forces between pairs of atoms within 9 Å were evaluated at every time step, and those between 9 and 14 Å every 10 steps. Coulomb interactions were calculated with the particle-mesh Ewald method²⁸ using a real-space cut-off of 9 Å and a grid spacing of 1.2 Å. The temperature was held constant at 1 bar using a Langevin thermostat with a friction of 1.0 ps⁻¹ and the pressure was maintained at either 1 bar or 600 bar using a Parrinello-Rahman barostat with a coupling time of 2.5 ps and using a compressibility of 4.5×10^{-5} bar⁻¹. RDCs were imposed as restraints via the orientational restraints feature of Gromacs.²⁹ The restraints were applied to a single copy (i.e., no time or ensemble averaging), with a force constant of 10.0 kJ mol⁻¹ Hz⁻². Briefly, in this scheme, the alignment tensor is always chosen to minimize the deviation of RDCs calculated from the current coordinates with respect to the experimental data and restraint forces are from the harmonic potential applied to the RMSD between experimental and calculated RDCs. A number of replicates of each simulation were run using different initial conditions, for a run time of up to 200 ns per run. The total amount of simulation time for each set of conditions and force field is given in Supporting Information Table S1. Conformations from the trajectories were clustered using the linkage algorithm and a 0.75 Å cut-off on backbone RMSD. At 1 bar, a single cluster accounted for 99% of the data, while at 600 bar two clusters (open and closed) accounted for 80% of the data between them, with the remaining clusters each containing less than 1.5% of the data. The central structures of these two clusters at 600 bar were used to define “open” and “closed” states.

RESULTS

To probe the effect of pressure on the protease structure, new sets of backbone ¹D_{NH} RDCs were measured under high-pressure conditions for the three different forms of the protease: inhibitor-free PR20, DMP323-bound PR, and inhibitor-free PR (Supporting Information Tables S1 and S2). Weak alignment of the NMR samples was achieved by the addition of a dilute solution of squalamine.³⁰ The partial alignment obtained with squalamine remained constant in the 1 bar–2.5 kbar pressure range (Supporting Information Fig. S2). Thus squalamine is an additional pressure-stable alignment medium.^{31,32} RDC measurements were carried out both 1 bar and at a pressure close to the midpoint of denaturation, where ~55% of the folded state is retained based on the relative intensities of the ¹H-¹⁵N cross peaks (Supporting Information Fig. S3), thereby maximizing the potential effects of pressure on the folded dimer. Significant ¹D_{NH} RDC differences were observed for the

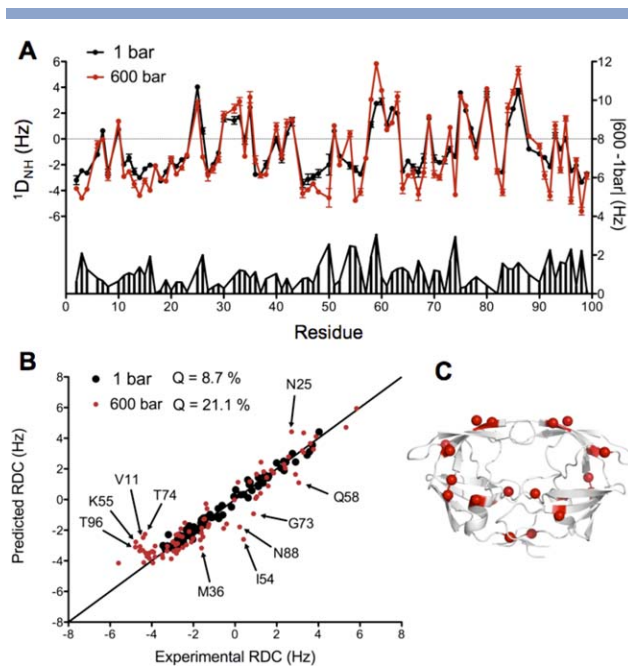


Figure 1

A: Backbone ¹D_{NH} RDCs measured for the inhibitor-free PR, at atmospheric (black) and high-pressure conditions (red). The absolute difference between the 1-bar and 600-bar RDC data sets is shown on the right y axis. **B:** Correlation between measured and predicted ¹D_{NH} RDCs of inhibitor-free PR, after refinement of the dimeric structure with the 1 bar data set, with the 1-bar RDCs in black and 600-bar RDCs in red. The largest outliers in the 600 bar data set are labeled in (B) and highlighted with red spheres on the HIV-1 PR structure in (C).

inhibitor-free PR throughout the protein, including the N-C termini, the active site, and the flap region [Fig. 1(A)]. These changes were associated with a significant decrease in the quality of the fit to the X-ray reference structure (PDB entry 3BVB),²³ with the Q-factor increasing from 22 to 48% for RDCs collected at 1 and 600 bar, respectively (Supporting Information Fig. S4). Differences in the quality of the fit could arise from local effects of pressure on the monomer subunit structures or from a change in the relative orientation of the subunits at the dimer interface. To distinguish these two effects, we first refined the dimeric X-ray reference structure (to which hydrogens had been added) against the 1-bar ¹D_{NH} RDCs, while keeping the non-H-atom coordinates tightly restrained to their crystallographically determined positions through a noncrystallographic symmetry term in the program XPLOR-NIH,³³ thereby reducing the effect of so-called structural noise.³⁴ The refined dimer yielded a Q-factor of 8.7% and, as expected, virtually the same number when fitting the monomeric subunit. The fit of the 600 bar RDCs to this refined structure also improves, from $Q = 0.48$ to $Q = 0.21$. Importantly, when fitting the 600 bar RDCs to the refined monomer structure, nearly the same fit quality is obtained ($Q = 0.21$)

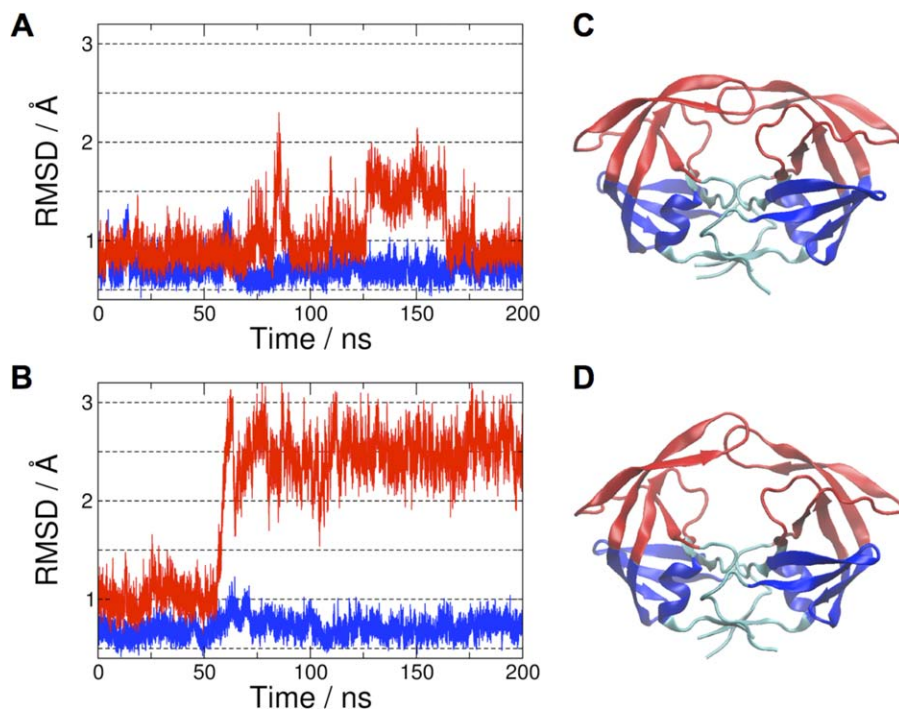


Figure 2

Backbone heavy atom root mean square deviation of representative simulations from reference structure 3BVB “core” region (residue 10–23 + 62–73 + 87–93) and “flap” region (residues 30–61 + 74–84). **A:** simulations at 1 bar, restrained to 1 bar RDC data. **B:** simulations at 600 bar, restrained to 600 bar RDC data. **C:** central structure of the “closed” cluster showing the “core” and “flap” regions in blue and red respectively. **D:** central structure of the “open” cluster showing the “core” and “flap” regions in blue and red, respectively. [Color figure can be viewed in the online issue, which is available at wileyonlinelibrary.com.]

[Fig. 1(B)], indicating that the decreased fit quality at 600 bar is not caused by a rearrangement of the dimer. Clear outliers in the fit of the 600 bar data [Fig. 1(B)] therefore must correspond to the local effects of pressure on the subunit structures. Residues with RDCs most affected by pressure are located in the N- and C-termini (residues V11 and T96), in the flaps (I54, K55, Q58) and in the active site (N25), but also in the “hinge” region of the protease (residues M36, G73, T74) [Fig. 1(B,C)].

To first characterize the pressure-induced structural changes observed for the inhibitor-free PR, we ran all-atom simulations in explicit solvent starting from the reference crystal structure 3BVB (after removing its ligand), in conjunction with a bias restraining the structure to the experimental RDCs measured at either 1 bar or 600 bar (Supporting Information Fig. S5 and Table S3). The TIP4P/2005 water model³⁵ was used for its ability to capture pressure-dependent equilibria,³⁶ in conjunction with the Amber ff99SBws protein force field optimized for this water model.²⁷ The simulation pressure was set to be the same as in experiment. All 10 simulations restrained to the 1-bar RDCs show flaps in a closed conformation, with a root mean square deviation (RMSD) <1 Å to the “core” and “flap” regions of the reference 3BVB structure for all runs [Fig. 2(A); Support-

ing Information Fig. S6], thereby confirming that the closed flap conformation constitutes the preferred conformation of the inhibitor-free PR at atmospheric pressure.²⁰ The simulations restrained to the 600 bar RDCs resulted in significant conformational changes in the flap region, with a final RMSD of ~2.5 Å from 3BVB [Fig. 2(B) and Supporting Information Fig. S7]. Inspection of the corresponding high-pressure trajectories shows a cooperative, two-state switch from the closed to a wide-open flap conformation. [Fig. 2(D)]. The “open” and “closed” reference structures shown in Figure 2(C,D) are based on a cluster analysis of the simulation trajectories, with the corresponding clusters accounting for ~80% of all data at 600 bar and >99% at 1 bar. Interestingly, we found that the central structure of the “open” cluster presents some significant differences in the flap region with the X-ray structure of the multi drug-resistant mutant PR20³⁷ even though both structures show a similar degree of opening (Supporting Information Fig. S8).

Similar results are obtained in alternate trajectories generated with the CHARMM 36 force field³⁸ and TIP3P water³⁹ (Supporting Information Fig. S9), showing that these results are not force-field dependent. Additional simulations at 1 bar, restrained to the 600-bar RDCs, again showed a transition to a more open

structure; similarly, simulations at 600 bar restrained to 1-bar RDCs remain in the closed conformation (Supporting Information Figs. S10 and S11). It is clear from the above that the results are primarily driven by the experimental restraints, rather than by the pressure in the simulation. Nonetheless, in accordance with Le Chatelier's principle, we found that the opening of the flaps at high pressure is driven by a reduction of the protein partial molar volume. We determine the difference of partial molar volumes at a given pressure as $\Delta V_m = N_A(V_O - V_C)$, where V_O and V_C are the average system volumes when the protein is in the open and closed states respectively and N_A is Avogadro's number (the number of water molecules being fixed). Here, we define "closed" states as those within 1.3 Å backbone RMSD of the 3BVB structure and "open" as those with RMSD from 3BVB >1.6 Å, yielding a difference of partial molar volume of $-29(11)$ and $-48(8)$ cm³ mol⁻¹ at 1 and 600 bar, respectively. Using these as lower and upper bounds, we estimate that 600 bar pressure should stabilize the open conformation of the flaps relative to the closed one by between -1.7 and -2.9 kJ mol⁻¹, an appreciable difference considering the relatively small pressure applied. Thus, by driving the conformational change using experimental data recorded at different pressures, we obtain a self-consistent change in simulation volume, indicating that this partial unfolding is also favored by high pressure in the context of the simulation force field.

The opening of the protease flaps with pressure explains the large change of RDCs for residues in the flaps (I54, K55) and in the adjoining hinge region (M36, Q58). However, there are several residues in the body of the protein that also exhibit substantial RDC changes with increased pressure: V11, G73, T74, and N88. Next to the larger scale conformational transitions associated with flap opening, pressure is expected to induce local effects caused by the burial of water molecules in interior cavities. To investigate such effects, we determined the changes in surface and buried water populations as a function of pressure (Supporting Information Table S4).

The largest changes are observed for the number of surface waters, with increases from closed to open conformations and from low to high simulation pressure. Both of these effects are to be expected, due respectively to the larger exposed surface area in the flap-open structure and to the increase in water density with pressure. The changes in the number of fully buried waters are much smaller, on the order of 1–3 additional water molecules at high pressure. Nonetheless, the differences exceed the simulation error. We determined for each heavy atom in the protein the average number of buried waters in contact with it at 1 bar and at 600 bar [Fig. 3(A)], showing a significant increase in the number of buried water molecules for atoms belonging to certain residues at high pressure. When focusing on the residues

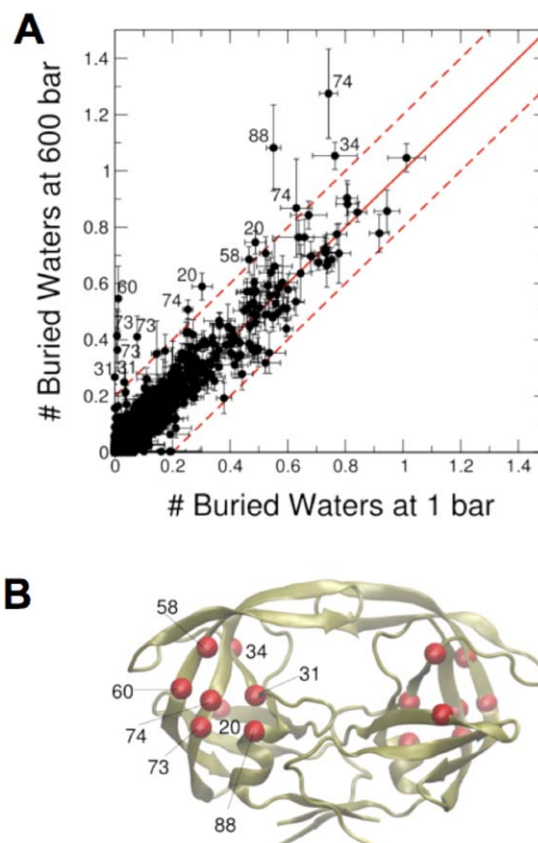


Figure 3

Changes in number of buried waters in contact with each protein heavy atom with pressure. **A:** Comparison between the average number of buried waters (as defined in text) in contact with each heavy atom in PR, at 1 bar and at 600 bar. The region between the broken red lines includes atoms with a difference of up to 0.2 water molecules at 1 bar and 600 bar. The heavy atoms lying outside this region are labeled with the number of the residue to which they belong. **B:** These residues are shown on the protease structure. [Color figure can be viewed in the online issue, which is available at wileyonlinelibrary.com.]

having atoms with an increase of more than 0.2 neighboring buried water molecules between the 1-bar and 600-bar structures, i.e. residues 20, 31, 34, 58, 60, 73, 74, and 88, we find that many of these are found clustered in the same region of the protein [Fig. 3(B)]. There is also a substantial overlap with the residues in the core of the protein with largest pressure-induced RDC changes, namely 11, 73, 74, 88. This suggests that although the absolute change in the number of buried waters is small, they appear to be related to the localized changes in RDC remote from the flap/hinge or terminal regions of the dimer. Overall, these results show a higher degree of water penetration in the trajectories restrained to the 600 bar RDCs compared with those restrained to the 1 bar data, and are consistent with a general mechanism of pressure-induced penetration of water molecules that destabilizes the native state, thereby leading to the complete unfolding of the protein.

In contrast to the free PR, the much smaller pressure-induced RDC changes measured for the DMP-bound PR and the free PR20 (Supporting Information Fig. S12A and B) suggest that these latter systems undergo a much more cooperative unfolding transition than free PR, with no detectable intermediate state. The drug-resistant mutant PR20 already adopts the open-flap conformation at atmospheric pressure,²⁰ such that its lowest free energy conformer already corresponds to the lower volume state of the native dimer. For the inhibitor-bound PR, the more cooperative unfolding likely arises from stabilization of the flap tips in the DMP-bound state. The structures of the DMP323-PR complex have indeed shown that the I50/I50' amide protons of the protease are hydrogen bonded with the urea oxygen of DMP323,²¹ thereby providing a direct coupling between the active site interface (residues 25–27) and the tips of the flaps (residues 49–51).

CONCLUSIONS

In summary, we have shown that the balance between the closed-flap and open-flap conformers is perturbed by high pressure, with the wide-open flap conformation becoming significantly more populated. In view of these results, the NMR relaxation data reported by Freedberg *et al.*⁴⁰ can possibly be interpreted as reflecting rapid transitions between closed and a small population of wide-open conformations, rather than between semi-open and wide-open conformations. In contrast to the inhibitor-free PR, little effect of pressure on the RDCs was observed for the inhibitor-free PR20 and the DMP323-bound PR, suggesting that both drug-resistance mutations and ligand binding can profoundly modify the folding free-energy landscape of mature HIV-1 protease. This study illustrates how the measurement of RDCs, combined with a mild and fully reversible pressure perturbation, in conjunction with advanced MD sampling methods can be used to describe low lying intermediate states in the folding energy landscape of a globular protein.

ACKNOWLEDGMENT

This study used the high-performance computational capabilities of the Biowulf Linux cluster at the National Institutes of Health, Bethesda, Md. (<http://biowulf.nih.gov>).

REFERENCES

1. Akasaka K. Probing conformational fluctuation of proteins by pressure perturbation. *Chem Rev* 2006;106:1814–1835.
2. Neudecker P, Robustelli P, Cavalli A, Walsh P, Lundstrom P, Zarrine-Afsar A, Sharpe S, Vendruscolo M, Kay LE. Structure of an intermediate state in protein folding and aggregation. *Science* 2012;336:362–366.
3. Sareth S, Li H, Yamada H, Woodward CK, Akasaka K. Rapid internal dynamics of BPTI is insensitive to pressure. (15)N spin relaxation at 2 kbar. *FEBS Lett* 2000;470:11–14.
4. Korzhnev DM, Bezsonova I, Evancin F, Taulier N, Zhou Z, Bai Y, Chalikian TV, Prosser RS, Kay LE. Probing the transition state ensemble of a protein folding reaction by pressure-dependent NMR relaxation dispersion. *J Am Chem Soc* 2006;128:5262–5269.
5. Fuentes EJ, Wand AJ. Local stability and dynamics of apocytochrome b562 examined by the dependence of hydrogen exchange on hydrostatic pressure. *Biochemistry* 1998;37:9877–9883.
6. Roche J, Dellarole M, Caro JA, Guca E, Norberto DR, Yang Y, Garcia AE, Roumestand C, Garcia-Moreno B, Royer CA. Remodeling of the folding free energy landscape of staphylococcal nuclease by cavity-creating mutations. *Biochemistry* 2012;51:9535–9546.
7. Nisius L, Grzesiek S. Key stabilizing elements of protein structure identified through pressure and temperature perturbation of its hydrogen bond network. *Nat Chem* 2012;4:711–717.
8. Roche J, Ying J, Maltsev AS, Bax A. Impact of hydrostatic pressure on an intrinsically disordered protein: a high-pressure NMR study of alpha-synuclein. *ChemBiochem* 2013;14:1754–1761.
9. Akasaka K, Li H. Low-lying excited states of proteins revealed from nonlinear pressure shifts in 1H and 15N NMR. *Biochemistry* 2001;40:8665–8671.
10. Kitahara R, Yokoyama S, Akasaka K. NMR snapshots of a fluctuating protein structure: ubiquitin at 30 bar–3 kbar. *J Mol Biol* 2005;347:277–285.
11. Prestegard JH, Bougault CM, Kishore AL. Residual dipolar couplings in structure determination of biomolecules. *Chem Rev* 2004;104:3519–3540.
12. Bax A, Grishaev A. Weak alignment NMR: a hawk-eyed view of biomolecular structure. *Curr Opin Struct Biol* 2005;15:563–570.
13. Kremer W, Arnold MR, Brunner E, Schuler B, Jaenicke R, Kalbitzer HR. High pressure NMR spectroscopy and its application to the cold shock protein *TmCsp* derived from the hyperthermophilic bacterium *Thermotoga maritima*. In: Winter R, editors. *Advances in High Pressure Bioscience and Biotechnology II*. Berlin: Springer Verlag; 2003. pp 101–112.
14. Raman S, Lange OF, Rossi P, Tyka M, Wang X, Aramini J, Liu G, Ramelot TA, Eletsky A, Szyperski T, Kennedy MA, Prestegard J, Montelione GT, Baker D. NMR structure determination for larger proteins using backbone-only data. *Science* 2010;327:1014–1018.
15. Montalvo RW, De Simone A, Vendruscolo M. Determination of structural fluctuations of proteins from structure-based calculations of residual dipolar couplings. *J Biomol NMR* 2012;53:281–292.
16. De Simone A, Montalvo RW, Dobson CM, Vendruscolo M. Characterization of the interdomain motions in hen lysozyme using residual dipolar couplings as replica-averaged structural restraints in molecular dynamics simulations. *Biochemistry* 2013;52:6480–6486.
17. De Simone A, Aprile FA, Dhulesia A, Dobson CM, Vendruscolo M. Structure of a low-population intermediate state in the release of an enzyme product. *eLIFE* 2015;2015:e02777.
18. Day R, Paschek D, Garcia AE. Microsecond simulations of the folding/unfolding thermodynamics of the Trp-cage miniprotein. *Proteins* 2010;78:1889–1899.
19. Louis JM, Ishima R, Torchia DA, Weber IT. HIV-1 protease: structure, dynamics and inhibition. *Adv Pharmacol* 2007;55:261–298.
20. Roche J, Louis JM, Bax A. Conformation of inhibitor-free HIV-1 protease derived from NMR spectroscopy in a weakly oriented solution. *ChemBioChem* 2015;16:214–218.
21. Lam PY, Jadhav PK, Eyermann CJ, Hodge CN, Ru Y, Bacheler LT, Meek JL, Otto MJ, Rayner MM, Wong YN, et al. Rational design of potent, bioavailable, nonpeptide cyclic ureas as HIV protease inhibitors. *Science* 1994;263:380–384.
22. Louis JM, Aniana A, Weber IT, Sayer JM. Inhibition of autoprocessing of natural variants and multidrug resistant mutant precursors of HIV-1 protease by clinical inhibitors. *Proc Natl Acad Sci U S A* 2011;108:9072–9077.

23. Sayer JM, Liu F, Ishima R, Weber IT, Louis JM. Effect of the active site D25N mutation on the structure, stability, and ligand binding of the mature HIV-1 protease. *J Biol Chem* 2008;283:13459–13470.
24. Fitzkee NC, Bax A. Facile measurement of ^1H - ^{15}N residual dipolar couplings in larger perdeuterated proteins. *J Biomol NMR* 2010;48:65–70.
25. Hess B, Kutzner C, Van der Spoel D, Lindahl E. GROMACS4: Algorithms for highly efficient, load-balanced, and scalable molecular simulation. *J Chem Theory Comput* 2008;4:435–447.
26. Hornak V, Abel R, Okur A, Strockbine B, Roitberg A, Simmerling C. Comparison of multiple AMBER force-fields and development of improved protein backbone parameters. *Proteins* 2006;65:712–725.
27. Best RB, Zheng W, Mittal J. Balanced protein-water interactions improve properties of disordered proteins and non-specific protein association. *J Chem Theory Comput* 2014;10:5113–5124.
28. Darden T, York D, Pedersen L. An N -log(N) method for Ewald sums in large systems. *J Chem Phys* 1993;103:8577–8592.
29. Hess B, Scheek RM. Orientation restraints in molecular dynamics simulations using time and ensemble averaging. *J Magn Reson* 2003;164:19–27.
30. Maltsev AS, Grishaev A, Roche J, Zasloff M, Bax A. Improved cross validation of a static ubiquitin structure derived from high precision residual dipolar couplings measured in a drug-based liquid crystalline phase. *J Am Chem Soc* 2014;136:3752–3755.
31. Fu YN, Wand AJ. Partial alignment and measurement of residual dipolar couplings of proteins under high hydrostatic pressure. *J Biomol NMR* 2013;56:353–357.
32. Sibille N, Dellarole M, Royer C, Roumestand C. Measuring residual dipolar couplings at high hydrostatic pressure: robustness of alignment media to high pressure. *J Biomol NMR* 2014;58:9–16.
33. Schwieters CD, Kuszewski JJ, Tjandra N, Clore GM. The Xplor-NIH NMR molecular structure determination package. *J Magn Reson* 2003;160:65–73.
34. Zweckstetter M, Bax A. Evaluation of uncertainty in alignment tensors obtained from dipolar couplings. *J Biomol NMR* 2002;23:127–137.
35. Abascal JLF, Vega C. A general purpose model for the condensed phases of water: TIP4P/2005. *J Chem Phys* 2005;123:234505
36. Best RB, Miller C, Mittal J. Role of solvation in pressure-induced helix stabilization. *J Chem Phys* 2014;141:22D522
37. Agniswamy J, Shen CH, Aniana A, Sayer JM, Louis JM, Weber IT. HIV-1 protease with 20 mutations exhibits extreme resistance to clinical inhibitors through coordinated structural rearrangements. *Biochemistry* 2012;51:2819–2828.
38. Best RB, Zhu X, Shim J, Lopes P, Mittal J, Feig M, MacKerell AD, Jr. Optimization of the additive CHARMM all-atom protein force field targeting improved sampling of the backbone ϕ , ψ and side-chain χ_1 and χ_2 dihedral angles. *J Chem Theory Comput* 2012;8:3257–3273.
39. Jorgensen WL, Chandrasekhar J, Madura JD. Comparison of simple potential functions for simulating liquid water. *J Chem Phys* 1983;79:926–935.
40. Freedberg DI, Ishima R, Jacob J, Wang YX, Kustanovich I, Louis JM, Torchia DA. Rapid structural fluctuations of the free HIV protease flaps in solution: relationship to crystal structures and comparison with predictions of dynamics calculations. *Protein Sci* 2002;11:221–232.